ISSN 1070-3284, Russian Journal of Coordination Chemistry, 2023, Vol. 49, No. 11, pp. 753–764. © Pleiades Publishing, Ltd., 2023.

Electronic Structures and Photo-Induced Geometry Distortion of Dinuclear Platinum(II) Complexes Featuring Janus-Type N-Heterocyclic Carbenes: A Theoretical Study

Kieu Thanh Canh[a], Phung Thi Thanh Hien[b], Nguyen Thi Thanh Huyen[c], and Nguyen Van Ha[b, *]

[a] *Tran Quoc Tuan University —First Army Academy, Co Dong, Son Tay, Hanoi, 12700 Vietnam*

[b] *Faculty of Chemistry, VNU University of Science, Vietnam National University, Hoan Kiem, Hanoi, 11021 Vietnam*

[c] *Hanoi National University of Education, Cau Giay, Hanoi, 11300 Vietnam*

**e-mail: nguyenvanha@vnu.edu.vn*

Received January 23, 2023; revised May 2, 2023; accepted May 19, 2023

Abstract—A series of neutral and anionic platinum(II) complexes bearing Janus-type N-Heterocyclic carbenes (NHC) with different extents of π conjugation were constructed theoretically by bridging two cyclometallated platinum(II) centers using diNHC linkers. The diNHCs bind to Pt(II) in either in monodentate (neutral complex **I**, **II**) or bidentate (anionic complex **III**–**V**) fashion. Structures of all complexes were first optimized. Single point and TD-DFT calculations have been carried out using the gas-phased optimized geometries to gain insight into their electronic structures, possible electronic transitions, and to probe the influence of diNHC ligand design on the photo-responsiveness of the complexes. The response of complexes **I**–**III** is limited to UV light; however, complexes **IV** and **V**, which contain cyclometallated diNHCs, exhibit absorption bands in the visible region. Additionally, the emissive triplet excited state and the metal-center triplet excited states (^{3}MC) were also investigated. Interestingly, the results suggest that the internal conversion triplet excited state to ^{3}MC in **I** and **III**, which induces significant coordination geometry distortion, is energetically favorable for complexes **I** and **III** suggesting potentially photo-enhanced reactivities of these two complexes.

Keywords: N-heterocyclic carbene, Janus-type NHC, cyclometallated Pt(II), electronic structures, photo-induced geometry distortion and ligand dissociation

DOI: 10.1134/S1070328423600043

INTRODUCTION

Platinum complexes have always been of particular interests in coordination chemistry owing to their many successes in pharmaceutical research as anticancer drugs, such as cis-platin, oxaliplatin, nedaplatin of platinum(II) or platinum(IV) complex satraplatin [1–3]. Additionally, platinum complexes have also been recognized as promising scaffolds for the developments photo-responsive materials [4, 5]. The heavy platinum(II) center with strong spin-orbit coupling facilitates the singlet-triplet (S-T) intersystem crossing, leading to better quantum yields of platinum complexes compared to classical organic materials. In parallel, excitation of some metal complexes, such as ruthenium and iridium, can result in the formation of metal-center triplet excited states (^{3}MC), facilitating ligand dissociations to generate the coordinatively unsaturated and more reactive species [6–9]. Photo-induced ligand dissociations are of great interest due to their potential application in photo-activated chemotherapy (PACT) [10–12]. We notice that, while photo-activatable octahedral platinum(IV) complexes have been extensively explored for the development of prodrugs [13, 14] photo-activation of platinum(II) complexes remain largely unexplored.

In the recent years, N-heterocyclic carbene (NHC) ligands have emerged into an important class of ligands for inorganic chemistry [15–19]. Their modular syntheses allow convenient access to NHC complexes of transition metals with different architectures, including mononuclear complexes [17], multiple homo/heteronuclear complexes [18–21] or 3-D structures [4, 5]. A large number of metal-NHCs have also demonstrated potential applications in various fields. For example, complexes bearing ligand with tunable stereoelectronic properties are excellent catalysis toward various chemical transformations [15, 22]. A number of mono and multinuclear complexes of NHCs display promising biological activities [23–25]. In addition, NHC complexes bearing extended π-conjugation systems are also a vital platform for the design and development of photo-responsive luminescent complexes [17, 26–28].

Despite the success of the two classes of compounds, the exploration of photo-responsive platinum(II) NHC complexes as photo-activatable drug candidates for application in photodynamic therapy remains almost unexplored [29]. A strong foundation in understanding of the electronic structures and behavior of photo-excited states of platinum(II) complexes is crucial for the creating effective designs. To support this premise, we reported in this work our theoretical study on both the ground and excited states of platinum(II) complexes featuring Janus-Type N-Heterocyclic carbenes. Structures of the dinuclear platinum(II) complexes of Janus-type NHC linkers C1C (**I**), C2C (**II**), CC1CC (**III**), CC2CC (**IV**) and CC2FCC (**V**) with numbering scheme for key atoms are listed in Scheme 1.

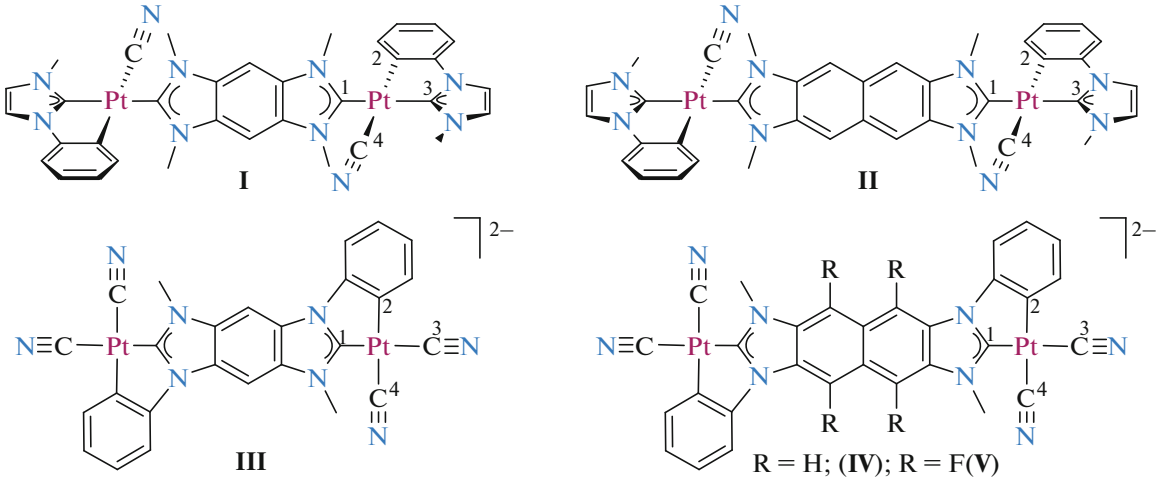

Scheme 1.

EXPERIMENTAL

Structures of all the complexes were first optimized using Gaussian® 16 software. Several functionals (B3LYP] [30], B3PW91 [31] and BPV86 [32]) and basis sets (SDD [33], LANL2DZ [34], 6-31G(d) [35]) combinations were tested to find the model which best describe the molecules. Nature of the stationary optimized points was confirmed to represent minima on energy potential surface by frequency analysis. Theoretically calculated infrared spectra of the complexes were generated using a 0.96 conversion factor. Using the best combination of functionals and basis set, electronic structures and Kohn-Sham orbitals were calculated. TD-DFT calculations were also performed to calculate vertical excitation energies. Geometries of the emissive excited states of the complexes (denoted as **I***–**V***) were optimized using unrestricted calculations starting from the ground state optimized structures. Frequency checks were also carried out to confirm that optimized structures were indeed the minima. It has been noted that the triplet metal center (^{3}MC) dd excited states are often accompanied by a severe structural distortion from the ground states [36, 37]. We were able to locate the ^{3}MC excited states using optimizations started with structures, where the cyanides ligands were slightly bend out of coordination plane.

RESULTS AND DISCUSSIONS

Structure and geometry of the complexes. Geometries of all complexes were first optimized in gas-phase conditions. To select the combination of functional and basis set which was most suitable for describing the above molecules, initial tests were carried out for complex **IV**, whose similar structure (complex **IVR**, Scheme 2) has been experimentally determined by single crystal X-ray diffraction [38]. Several combinations of functionals and basis sets, namely B3PW91 (SDD/6-31G(d)) (**a**); B3PW91 (LANL2DZ/6-31G(d)) (**b**); B3LYP (SDD/6-31G(d)) (**c**); B3LYP (LANL2DZ/6-31G(d)) (**d**); and BPV86 (SDD/6-31G(d)) (**e**) were utilized to optimize the structure of **IV**. Structural parameters, including key bond lengths and angles, of the optimized structures were compared to the reported values (**IVR**) (Table 1). In general, all the tested combinations can give satisfactory models of the complexes. Close examination reveals that while calculations using B3LYP functionals (c, d) slightly overestimate the bond distances, calculation using B3PW91 and BPV86 functionals closely resemble the experimental structure. For further analysis, all calculations were carried using B3PW91 (SDD/6-31G(d)) combination.

Table 1. Selected bond length (Å) and bond angle (deg) for optimized geometries of the complexes

Structure	Bond length, Å				Bond angle, (deg		
	Pt–C(1)	Pt–C(2)	Pt–C(3)	Pt–C(4)	C(1)PtC(2)	C(1)PtC(3)	C(2)PtC(4)
IVR	2.008	2.052	2.003	2.025	79.0	172.3	176.9
IVa	2.011	2.055	2.003	2.026	79.2	171.3	178.3
IVb	2.009	2.049	1.999	2.029	79.3	171.4	178.4
IVc	2.027	2.069	2.016	2.043	79.1	171.3	178.0
IVd	2.025	2.063	2.013	2.047	79.3	171.4	178.2
IVe	2.014	2.066	2.005	2.028	79.3	171.2	178.1

Table 2. Selected bond length (Å) and bond angle (deg) for optimized geometries of **I**–**V**

Structure	Bond length, Å				Bond angle, deg			
	Pt–C(1)	Pt–C(2)	Pt–C(3)	Pt–C(4)	∠C(1)PtC(2)	C(2)PtC(3)	C(1)PtC(3)	C(2)PtC(4)
I	2.022	2.068	2.035	2.022	94.9	79.2	174.0	177.3
II	2.019	2.068	2.037	2.022	94.8	79.1	173.9	177.2
III	2.016	2.055	2.002	2.025	79.1	92.1	171.2	177.9
IV	2.011	2.055	2.003	2.026	79.2	92.1	171.3	178.3
V	2.010	2.051	2.002	2.029	79.0	92.1	170.9	178.2

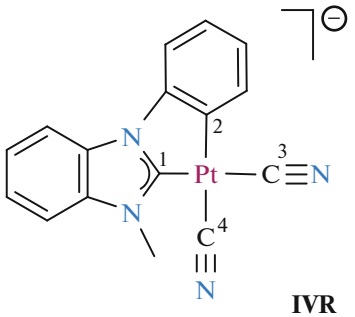

IVR

Scheme 2.

Using the B3PW91 (SDD/6-31G(d)) methodology, gas-phased optimized structure of all the complexes were obtained (Fig. 1). Selected bond lengths and angles are listed in Table 2. In general, the optimized geometries of the complexes show highly symmetrical structures. All the complexes possess centers of inversion, which coincide with the centers of the diNHC ligands. In addition, the coordination geometries of the platinum(II) centers are essentially square planar. In complexes **I** and **II**, the platinum(II) coordination planes are near perpendicular to the diNHC plane, forming dihedral angles of 80.4° (**I**) and 82.1° (**II**). Conversely, the Pt(II) coordination planes in complex **III**–**V** align with the diNHC plane and the entire fragments are coplanar. Perfect planarity is observed for structure of **III** and **IV**. On the other hand, due to steric effect caused by the larger florines (as compared to hydrogen), the phenyl rings bend slightly out of the diNHC plane, forming dihedral angle of 13.5°. All the Pt–C_{NHC} bond lengths are in the 2.010–2.035 Å range, which is close to reported values [39]. Slightly longer distances (2.051–2.068 Å) are observed for Pt–$C_{carbanion}$ bonds. In the structure of **III**–**V**, the distance between platinum(II) and the carbon of the cyanido ligands Pt–C(4) are slightly longer than the Pt–C(3), which agrees well with stronger *trans* effect exerted by the anionic carbanion compared to the neutral carbene carbon. The bidentate bite angles are in the range of 79.0°–79.2°, which is closed to the angle of 79.0° determined for **IVR** [40]. It should be noted that increasing the number of fused benzo-ring in the Janus-type diNHC from one in **I** (C1C), **III** (CC1CC) to two in **II** (C2C) and **IV**/**V** (CC2CC/CC2FCC) does not induce any significant changes in the bond lengths or bond angles around the platinum(II) centers.

Stretching vibration of the complexes. All the complexes bear cyanido ligands, whose vibrational absorptions are intense and well separated from the rest. Stretching frequencies of the CN ligands in the complexes are listed in Table 3. The cyanido ligands in **I** and **II** exhibit absorption bands at 2124 cm^{-1} in their theoretical IR spectra. Absorptions at slightly higher energy were observed for $C^3{\equiv}N$ and $C^4{\equiv}N$ in spectra of **III** (2149 and 2131 cm^{-1}), **IV** (2150, 2133 cm^{-1}) and **V** (2152 and 2135 cm^{-1}). Noted that, while the C(4)≡N

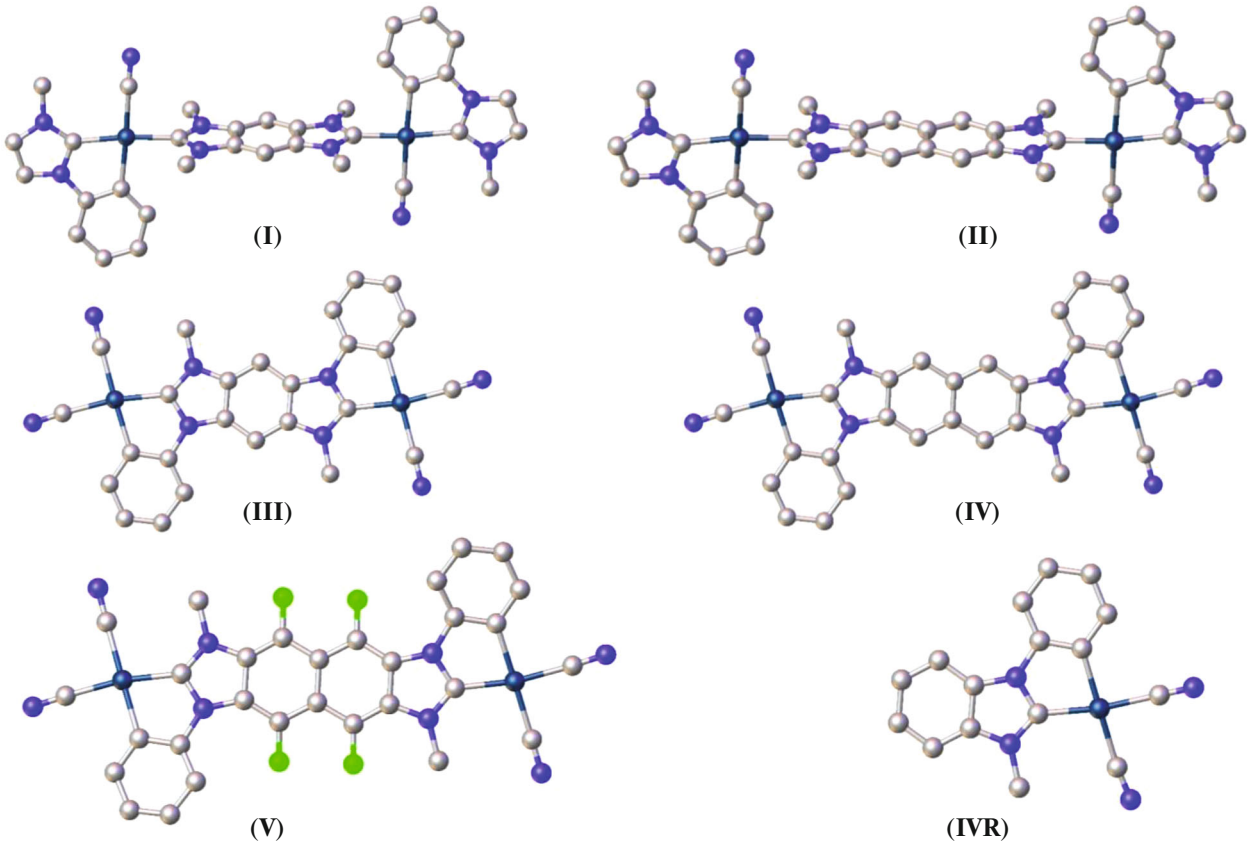

Fig. 1. Optimized structures of the neutral (**I**, **II**), dianionic (**III–V**) complexes and experimentally determined structure of anionic **IVR**.

are *trans* to the strong donor carbanion, the C(3)≡N ligands are *trans* to the less donating carbene. Therefore, it is reasonable that stretching frequency of C(3)≡N are higher compared to that of C(4)≡N. In addition, there values are somewhat comparable to the C≡N stretching frequency for the $[Pt(CN)_4]^-$ anionic complex (2118 cm^{-1}) [40].

Electronic structure of the complexes. To shed light on the electronic structure of the complexes, single point calculations were carried out using the optimized geometries. The surfaces of frontier molecular orbitals are presented in Fig. 2 along with definition of coordinates (Scheme 3). For complex **I**, the highest occupied molecular orbital HOMO, HOMO – 1 are degenerate and are primarily composed of π conjugation of the cyclometallated phenyl imidazoline-2-ylidene (ImPh) ligands with small contribution from the Pt(II) d_{yz} orbital. On the other hand, the LUMO orbital is primarily comprised of π* of the C1C bridging ligand with a small contribution of Pt(II) d_{xy} orbital. The LUMO + 1 is mainly derived from the π* of the cyclometallated ImPh ligands. For complex **II**, the HOMO and LUMO orbitals are essentially composed of π conjugation system of the C2C ligands, which is in line with the expectation that extending the π conjugation from C1C to C2C will reduce the HOMO−LUMO energy gap. Moreover, HOMO − 1 and LUMO + 1 are delocalized on the ImPh backbone with significant contribution from d_{yz} (for HOMO − 1) and d_{xz} (for LUMO + 1). Substantial changes in the electronic structure of the complexes were observed upon converting the bridging diNHC into cyclometallated ligands (i.e. CC1CC, CC2CC, CC2FCC).

Table 3. Stretching frequency of CN ligands in the complexes

Complex	$\nu_{C\equiv N}$ stretching frequency, cm^{-1}	
	C(3)≡N	C(4)≡N
I		2124
II		2124
III	2149	2131
IV	2150	2133
V	2152	2135

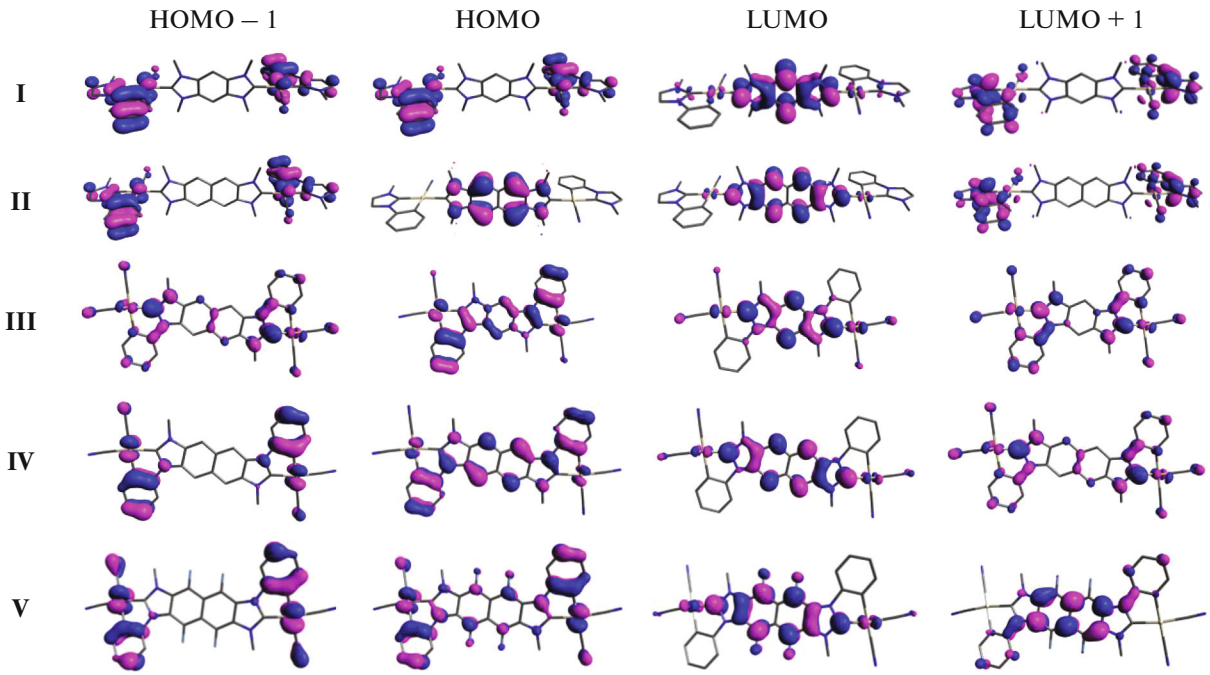

Fig. 2. Frontier orbitals of the complexes calculated at B3PW91/(SDD + 6-31G*) level (isovalue 0.035).

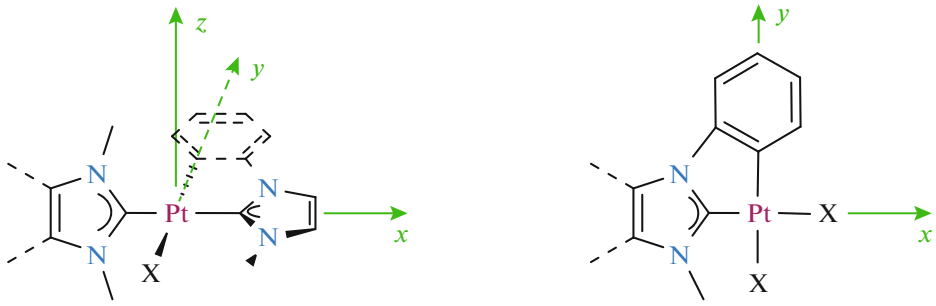

Scheme 3.

In complex **III**–**V**, the HOMO orbitals are delocalized over the entire CC1CC (**III**) and CC2CC (**IV**) ligands, including the carbanion phenyl ring. Small contributions from the Pt(II) d_{yz} orbitals are also evidenced. Fluorination of the bridging ligand (complex **V**) leads to a decrease in contribution of the fused benzo-ring to the HOMO. In addition, the HOMO − 1 orbitals of **III**–**V** share similar feature with that of complex **I** and **II**. These HOMO − 1 orbitals are primarily comprised of the π of the carbanion phenyl ring with substantial contribution from Pt(II) d_{yz} orbitals, and to a lesser extend, the π orbital of the cyanido ligand. On the other hand, the LUMO orbitals of complex **III**–**V** are centralized on the benzo-ring and the two heterocycle of the bridging diNHC cores. In addition, the LUMO + 1 orbitals for **III** and **IV** span over the entire molecules, showing contribution from the CC1CC (**III**) and CC2CC (**IV**) π* conjugation, Pt(II) d_{xz} and cyanido-π* orbitals.

Energy level of the frontier orbitals in the complexes are plotted in Fig. 3 for comparison. It can be seen that, addition of a benzo-ring to the C1C (**I**) to form C2C (**II**) ligands extends the π conjugation of the bridging ligands, and significantly reduces the diNHC π–π* gap. The π–π* gap sinkage leads to alteration in the nature of the HOMO orbitals from ImPh-based (in **I**) to C2C-based (in **II**). Though LUMO orbital of **III** has similar energy compared to that of complex **I**, the HOMO energy is relatively higher, which can be attributed to an increased Coulombic repulsion in the anionic complex **III**. Further extending the π-conjugation system results in a smaller HOMO–LUMO gap in **IV**. Moreover, the addition of fluorine atoms to the CC2CC ligand backbone stabilizes the LUMO and to

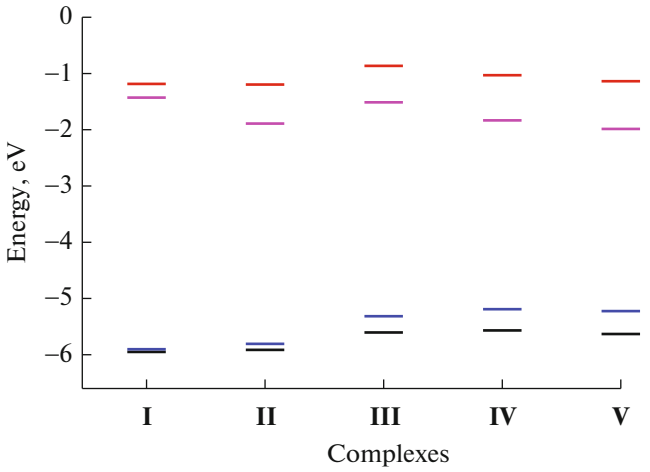

Fig. 3. Comparison energy level of frontier orbitals (HOMO-blue; HOMO − 1, black; LUMO, magenta; LUMO + 1, red).

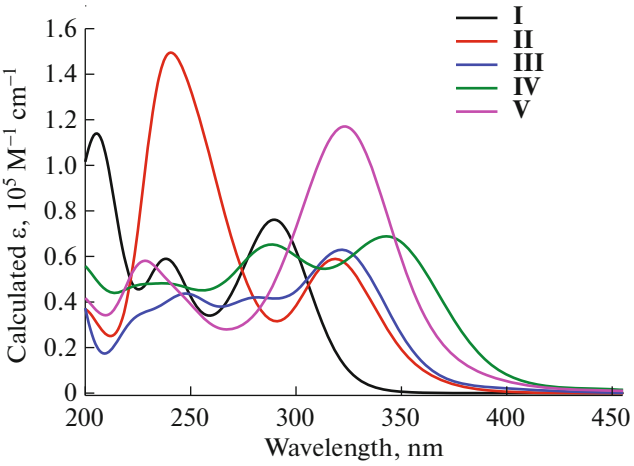

Fig. 4. Simulated UV-Vis absorption of the complexes.

a lesser extend the HOMO of **V** and therefore this complexes have the smallest HOMO−LUMO energy gap (Fig. 3).

Vertical excitation of the complexes. Electronic transitions of the complexes were investigated by TD-DFT calculation to gain understanding on their photophysical properties. The calculated vertical excitations are listed in Table 4 and simulated UV-Vis absorption spectra of the complexes in the 200−600 nm range are presented in Fig. 4. The data clearly show that complex **I** is not responsive to visible light, showing the lowest energy transition calculated at 323 nm with high extinction coefficient. This transition is originated from $\pi_{ImPh} \rightarrow \pi^*_{ClC}$ ligand-to-ligand charge transfer (LLCT), $\pi_{ImPh} \rightarrow \pi^*_{ImPh}$ intra-ligand charge transfer (ILCT) as well as metal *d*−*d* transitions and $d_{Pt(II)} \rightarrow \pi^*_{ClC}$ metal ligand charge transfer (MLCT) (Table 4, Fig. 4).

In the simulated UV-Vis spectrum of **II**, the intense absorption at 351 nm represents the lowest energy transition, which is predominantly C2C ILCT. Other higher energy absorption bands at 347 and 318 nm result from the mixing of C2C, ImPh intra-ligand charge transfer, Pt(II) $\rightarrow \pi^*_{C2C/ImPh}$ MLCT and metal center *d*−*d* transition. It is notable that neither of the complexes are responsive to visible light activations. In complex **III**, the design of the bridging ligand is changed by incorporating the phenyl π systems coplanar to the diNHC, resulting in the formation of CC1CC with a more extended π conjugation. As a consequence, the complex exhibits lowest energy transition at 387 nm, which is largely attributed to CC1CC ILCT with contribution from Pt(II) → CC1CC MLCT. This weak absorption band is accompanied by an intense absorption center at 326 nm, which originates from ILCT of the CC1CC ligand. Metal to ligand (Pt(II) → CC1CC) charge transfer is found at higher energy (322 nm), overlapping with Pt(II) *d*−*d* transition (Table 4). The additional fused benzo-ring in complex **IV** causes a lowering of the HOMO−LUMO gap, which shifts the lowest energy absorption to visible region. The simulated UV-Vis spectrum of conplex **IV** shows a weak absorption band at 432 nm. The band share similar feature with the lowest energy absorption of **III**, which is CC2CC ILCT with contribution from Pt(II) $\rightarrow \pi^*_{CC2CC}$ MLCT. All of the higher energy absorptions in these complex originate primarily from metal perturbed π → π* transition. Notably, a further shift into the visible region was successfully achieved by fluorinating the diNHC core. Although the absorption intensity is low, the fluorinated complex **V** exhibits a lowest energy absorption band centered at 447 nm, which is predominantly $\pi_{CC2FCC} \rightarrow \pi^*_{CC2FCC}$ intra-ligand charge transfer with substantial contribution from Pt(II) → π^*_{CC2FCC} MLCT.

Emissive triplet states of the complexes. It is well established that strong spin-orbit coupling of the platinum(II) center promote S → T singlet-triplet intersystem crossing, and platinum(II) complexes have a strong tendency to form triplet excited states. The triplet excited states can be emissive ^{3}MLCT, ^{3}ILCT or structurally distorted non-emissive metal centered (^{3}MC) ones and understanding their nature is helpful for exploring the potential applications of the complexes.

Optimization of the emissive triplet excited state was carried out using the same functional and basis sets, starting from the optimized ground state geometries. The optimized geometries (**I*−V***) of the complexes are presented in Fig. 5, along with their plots of spin density distributions, while selected structural

Table 4. Vertical excitation energies of **I**–**V**

E, nm[a]	Osc. Str[b]	Transitions	Con., %[c]	Assignment
		I		
323	0.0133	H → L	42	$\pi_{ImPh} + d_{yz} \rightarrow \pi^*_{C1C}$
		H-1 → L + 1	35	$\pi_{ImPh} + d_{yz} \rightarrow \pi^*_{ImPh} + d_{xz}$
		H → L + 2	20	$\pi_{ImPh} + d_{yz} \rightarrow \pi^*_{ImPh} + \pi^*_{C1C}$
307	0.010	H → L	53	$\pi_{ImPh} + d_{yz} \rightarrow \pi^*_{C1C}$
		H → L + 2	30	$\pi_{ImPh} + d_{yz} \rightarrow \pi^*_{ImPh} + \pi^*_{C1C}$
292	1.16	H-2 → L	88	$\pi_{ImPh} + d_{xy} \rightarrow \pi^*_{C1C}$
		II		
351	0.071	H → L	94	$\pi_{C2C} \rightarrow \pi^*_{C2C}$
347	0.010	H-2 → L	94	$\pi_{ImPh} + d_{yz} \rightarrow \pi^*_{C2C}$
319	0.326	H-3 → L	32	$\pi_{C2C} + d_{xy} \rightarrow \pi^*_{C2C}$
		H-2 → L + 2	30	$\pi_{ImPh} + d_{xy} \rightarrow \pi^*_{ImPh} + d_{xz}$
		H-1 → L + 1	30	$\pi_{ImPh} + d_{yz} \rightarrow \pi^*_{ImPh} + d_{xz}$
318	0.712	H-3 → L	54	$\pi_{C2C} + d_{xy} \rightarrow \pi^*_{C2C}$
		H-1 → L + 1	20	$\pi_{ImPh} + d_{yz} \rightarrow \pi^*_{ImPh} + d_{xz}$
		III		
387	0.039	H → L	94	$\pi_{CC1CC} + d_{yz} \rightarrow \pi^*_{CC1CC} + d_{xz}$
326	0.858	H-2 → L	93	$\pi_{CC1CC} + d_{xz} \rightarrow \pi^*_{CC1CC} + d_{xz}$
322	0.047	H-5 → L H-4 → L + 1	88 11	$d^2_z \rightarrow \pi^*_{CC1CC} + d_{xz}$
315	0.203	H-3 → L	79	$\pi_{CC1CC} + d_{yz} \rightarrow \pi^*_{CC1CC} + d_{xz}$
		H-1 → L + 1	9	$\pi_{CC1CC} + d_{yz} \rightarrow \pi^*_{CC1CC} + d_{xz}$
		IV		
432	0.032	H → L	100	$\pi_{CC2CC} + d_{yz} \rightarrow \pi^*_{CC2CC} + d_{xz}$
359	0.273	H-2 → L	87	$\pi_{CC2CC} + d_{xz} \rightarrow \pi^*_{CC2CC} + d_{xz}$
		H-1 → L + 1	6	$\pi_{CC2CC} + d_{yz} \rightarrow \pi^*_{CC2CC} + d_{xz}$
345	0.878	H-3 → L	90	$\pi_{CC2CC} + d_{xz} \rightarrow \pi^*_{CC2CC} + d_{xz}$

Table 4. (Contd.)

E, nm[a]	Osc. Str[b]	Transitions	Con., %[c]	Assignment
316	0.409	H-1 → L + 1	54	$\pi_{CC2CC} + d_{yz} \rightarrow \pi^*_{CC2CC} + d_{xz}$
		H → L + 2	34	$\pi_{CC2CC} + d_{yz} \rightarrow \pi^*_{CC2CC}$
		H-2 → L	6	$\pi_{CC2CC} + d_{xz} \rightarrow \pi^*_{CC2CC} + d_{xz}$
301	0.179	H → L + 2	35	$\pi_{CC2CC} + d_{yz} \rightarrow \pi^*_{CC2CC}$
		H-8 → L	34	$\pi_{CC2CC} \rightarrow \pi^*_{CC2CC} + d_{xz}$
V				
447	0.0164	H → L	95	$\pi_{CC2FCC} + d_{yz} \rightarrow \pi^*_{CC2FCC} + d_{xz}$
373	0.1236	H-2 → L	88	$\pi_{CC2FCC} + d_{xz} \rightarrow \pi^*_{CC2FCC} + d_{xz}$
348	0.0248	H-6 → L	82	$d^2_z \rightarrow \pi^*_{CC2FCC} + d_{xz}$
344	0.1095	H-3 → L	68	$\pi_{CC2FCC} + d_{xz} \rightarrow \pi^*_{CC2FCC} + d_{xz}$
327	1.6819	H → L + 2	54	$\pi_{CC2FCC} + d_{yz} \rightarrow \pi^*_{CC2FCC}$
		H-3 → L	22	$\pi_{CC2FCC} + d_{xz} \rightarrow \pi^*_{CC2FCC} + d_{xz}$
315	0.2210	H-1 → L + 1	57	$\pi_{CC2FCC} + d_{xz} \rightarrow \pi^*_{CC2FCC} + d_{xz}$

[a] Excitation energy; [b] oscillator strength; [c] contribution; [d] experimental UV absorption maxima.

parameters are presented in Table 5. In general, the triplet excited state optimized geometries display no significant rearrangement of the ligands with all the Pt(II) coordination planes remain essentially square planar. In the structures of **I*** and **II***, the coordination planes form dihedral angles of 75.8° and 87.4° (for **I***) and 86.5° and 86.5° (for **II***) with the diNHC mean planes. On the other hand, in the structures of complexes **III***–**V***, the diNHC and coordination planes are essentially coplanar. It should be noted that the structures of **II***, **IV*** and **V*** remain symmetrical, adopting nearly C_2 symmetry. These geometries show a slight elongation of the Pt–C_{diNHC} bond by 0.01–0.02 Å. For example, the length of Pt–C1 bonds are 2.019 Å (in **II**) and 2.010 Å (in **V**) while the values are 2.039 and 2.026 Å in **II*** and **V***, respectively (Table 5). The other bonds between Pt(II) and the other ligands remain relatively the same. On the other hand, complexes **I*** and **III*** loss their symmetry up on excitation giving complexes with two Pt(II) centers with non-identical geometries. In the structure of **I***, the Pt(1)–C(1) is drastically elongated, while Pt(1)–C(2) bond is significantly shorter compared to the respective bond in **I**. Similarly, a markedly shorter Pt(1)–C(2) bond is also observed in the structure of **III***. In all cases, the change in bond angle around the Pt(II) centers is insignificant.

Figure 5 also clearly shows that the spin density of **II***, **IV*** and **V*** is delocalized on the diNHC ligands with negligible contribution from the Pt(II) *d*-orbitals, and these states are assigned as intra-ligand charge transfer triplet states (^{3}ILCT). In sharp contrast, significant contribution from the *d*-orbital of one of the Pt(1) is evidenced for **I*** and **III***. In **I***, the triplet excited state arises from a metal-to-ligand charge transfer state (^{3}MLCT), showing spin density distributed over the ImPh ligand and the *d*-orbital of Pt(1) (spin density 0.26). A similar ^{3}MLCT nature of the triplet excited state for **III*** is also noticed, where Pt(1) *d*-orbital significantly contributes to the over all spin density in addition to that of the diNHC ligands. A spin density of 0.16 was observed for Pt(1).

It has been established that the excited platinum(II) complexes may be accessible to metal centered triplet excited state, and thereafter undergo ligand distortion [36, 37, 41]. We are able to locate the low-lying metal-centered triplet excited state (^{3}MC) for the complexes and the optimized structures for these ^{3}MC excited state are presented in Fig. 6. Spin density localizes on the Pt(1) was determined to be 1.29 (**I***), 1.23 (**II***), 0.71 (**III***), 1.33 (**IV***) and 1.31 (**V***). Additionally, representative spin density distribution for **III*** and **IV*** are plotted in Fig. 7.

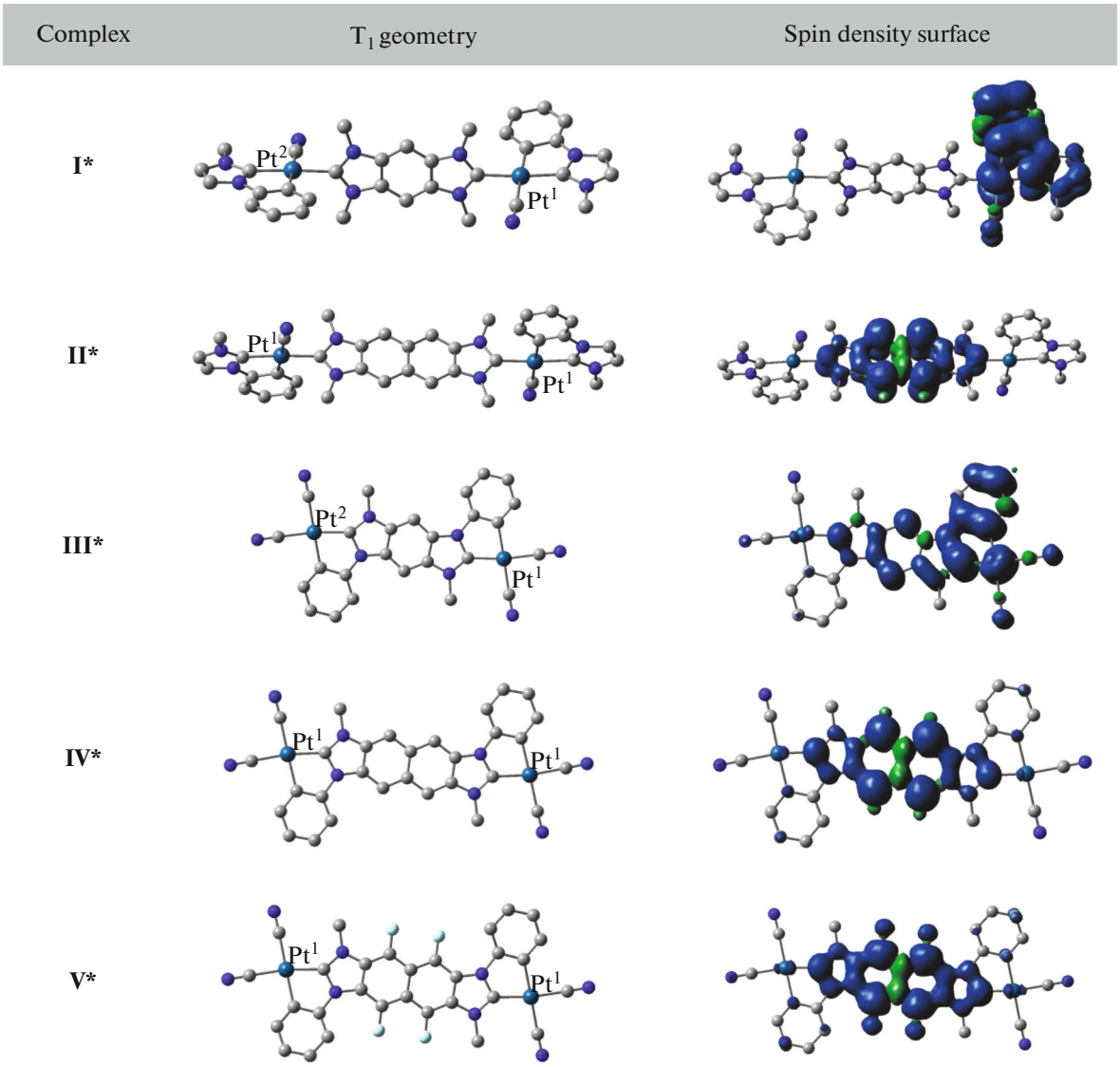

Fig. 5. Optimized lowest energy triplet excited state of the complexes and their spin density plots.

In general, these ^{3}MC excited states exhibit a heavily distorted coordination sphere. In each structure, one cyanido ligands, which is bonded to Pt^1 and in *trans* configuration with respect to the carbanion, significantly bends out of the plane form by Pt^1 and the three remaining donor atoms (Fig. 6). The C(2)Pt(1)C(4) bond angles are 94.7° (**I***, **II***), 104.1 (**III***), 104.5 (**IV***) and 107.3 (**V***). The energy levels of the ground and excited states are presented in Table 6 and a comparison between these states is presented in Fig. 8.

It can be observed that the ^{3}MC excited states of **I*** and **II***, as well as of **III***, **IV***, and **V***, exhibit a considerable similarity in their energy levels, due to the comparable ligand field strength between C1C, C2C, CC1CC, CC2CC, and CC2FCC. On the other hand, the ^{3}ML/ILCT excited state of **II***, **IV*** and **V*** are more stabilized compared to **I*** and **III***, which can be attributed to the more extensive π-conjugation of **C2C** in comparison to C1C and of CC2CC and CC2FCC compared to CC1CC. As a result, the ^{3}MC state of **I*** and **III*** lie at significantly lower energy levels than the respective ^{3}ML/ILCT states, indicating that the distortion induced by photoexcitation is energetically favored. Investigating the thermodynamic factor may be worthwhile for developing and designing of complexes, which are capable of undergoing photo-induced ligand dissociation, thereby enhancing their interaction with biomolecules.

Electronic structures of five neutral and anionic dinuclear platinum(II) complexes bearing bridging diNHC ligands have been investigated. The initial cal-

Table 5. Selected bond length (Å) and bond angle (deg) for ILCT[3] optimized geometries of the complexes

Structure	Bond length, Å				Bond angle, deg			
	Pt–C(1)	Pt–C(2)	Pt–C(3)	Pt–C(4)	C(1)PtC(2)	C(2)PtC(3)	C(1)PtC(3)	C(2)PtC(4)
I*	2.048 2.034	2.011 2.067	2.004 2.042	2.029 2.022	94.3 93.5	79.9 79.1	174.2 172.6	178.1 178.2
II*	2.039	2.067	2.041	2.021	93.4	79.1	172.6	178.2
III*	1.999 2.021	2.016 2.054	2.005 1.999	2.027 2.025	79.7 79.2	93.1 92.8	172.8 171.9	178.6 178.7
IV*	2.024 2.026	2.053 2.053	2.000 2.000	2.023 2.023	78.9 78.9	92.8 92.8	181.7 171.7	178.4 178.4
V*	2.026	2.051	1.997	2.026	78.8	92.9	171.5	178.4

culations tested various functional and basis sets and suggested that the B3PW91/(6-31G(d)/SDD) combination could best reproduce the structures of the cyclometallated platinum(II)-NHC complexes. Single point calculations revealed the nature of frontier orbitals of the complexes. It was noted that by integrating the cyclometallated phenyl to the diNHC ligands, extending the π-conjugation to the entire molecules, it is possible to shift the lowest absorption band of complexes **IV** and **V** toward the visible region. Interestingly, study on triplet excited state of the complexes suggest that the internal conversion from ^{3}MLCT to ^{3}MC states are energetically favorable in case of complex **I** and **III**, accompanied by heavily distorted coordination geometry. This phenomenon may have implication in exploring this platform to develop pho-

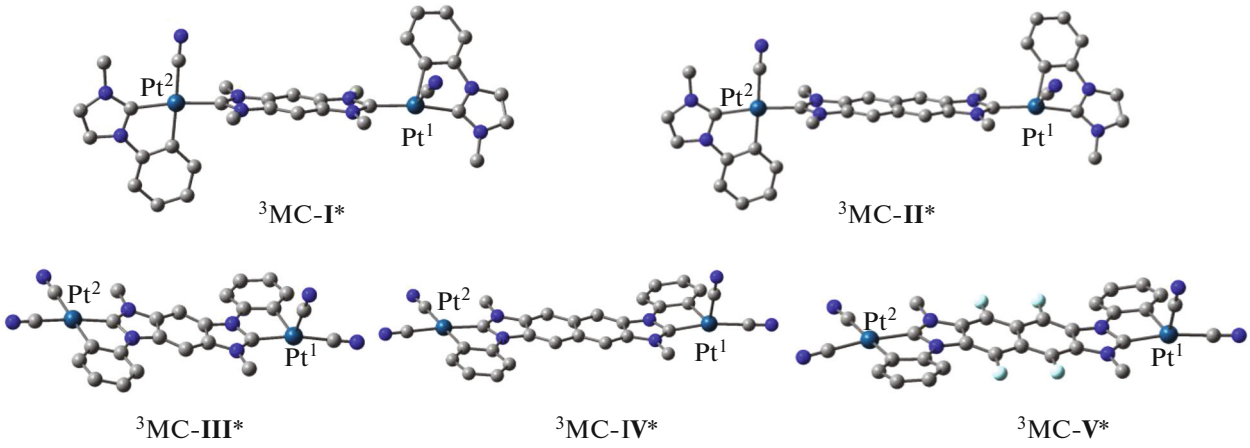

Fig. 6. Optimized geometries for ^{3}MC excited state of the complexes.

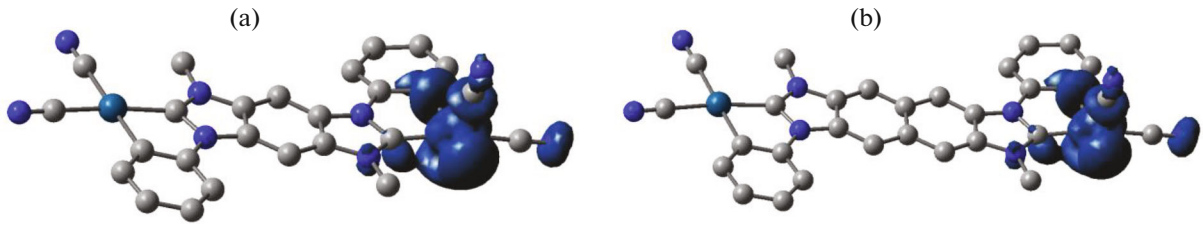

Fig. 7. Spin density distribution for ^{3}MC-**III*** (a) and ^{3}MC-**IV*** (b) (isovalue 0.005).

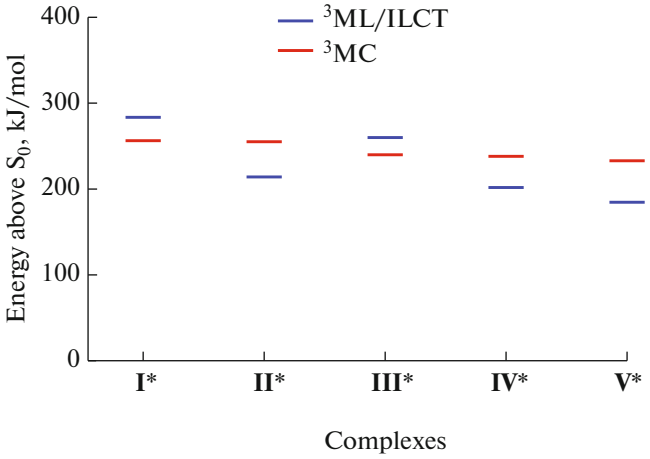

Fig. 8. Energy comparison for triplet excited state energy for the complexes.

Table 6. Energy level of the ground and excited states of the complexes

Complex	Energy level, Ha		
	S_0	^{3}ML/ILCT	^{3}MC
I	−2100.73	−2100.63	−2100.64
II	−2254.31	−2254.23	−2254.22
III	−1677.14	−1677.04	−1677.05
IV	−1830.72	−1830.64	−1830.63
V	−2227.46	−2227.39	−2227.37

toactivatable complexes for potential application in photo-activated chemotherapy.

FUNDING

This research is funded by the Vietnam National University, Hanoi (VNU) under project number QG.20.16.

CONFLICT OF INTEREST

The author of this work declares that they has no conflicts of interest.

REFERENCES

1. Miskowski, V.M., Houlding, V.H., Che, C.M., and Wang, Y., *Inorg. Chem.*, 1993, vol. 32, p. 2518. https://doi.org/10.1021/ic00063a052
2. Chan, A.K.W. and Yam, V.W.W., *Acc. Chem. Res.*, 2018, vol. 51, p. 3041. https://doi.org/10.1021/acs.accounts.8b00339
3. Vu, A.T., Santos, D.A., Hale, J.G., and Garner, R.N., *Inorg. Chim. Acta*, 2016, vol. 450, p. 23. https://doi.org/10.1016/j.ica.2016.05.007
4. Martínez-Agramunt, V., Ruiz-Botella, S., and Peris, E., *Chem. Eur. J.*, 2017, vol. 23, p. 6675. https://doi.org/10.1002/chem.201700703
5. Horiuchi, S., Moon, S., Ito, A., et al., *Angew. Chem. Int. Ed.*, 2021, vol. 60, p. 10654. https://doi.org/10.1002/anie.202101460
6. Loftus, L.M., Rack, J.J., and Turro, C., *Chem. Commun.*, 2020, vol. 56, p. 4070. https://doi.org/10.1039/C9CC10095D
7. Betanzos-Lara, S., Salassa, L., Habtemariam, A., et al., *Organometallics*, 2012, vol. 31, p. 3466. https://doi.org/10.1021/om201177y
8. Nisbett, K., Tu, Y.J., Turro, C., et al., *Inorg. Chem.*, 2018, vol. 57, p. 231. https://doi.org/10.1021/acs.inorgchem.7b02398
9. Vu, A.T., Santos, D.A., Hale, J.G., and Garner, R.N., *Inorg. Chim. Acta.*, 2016, vol. 450, p. 23. https://doi.org/10.1016/j.ica.2016.05.007
10. Morales, K., Samper, K.G., Pena, Q., et al., *Inorg. Chem.*, 2018, vol. 57, p. 15517. https://doi.org/10.1021/acs.inorgchem.8b02854
11. Monro, S., Colon, K.L., Yin, H., et al., *Chem. Rev.*, 2019, vol. 119, p. 797. https://doi.org/10.1021/acs.chemrev.8b00211
12. Zhao, Y., Roberts, G.M., Greenough, S.E., et al., *Angew. Chem. Int. Ed.*, 2012, vol. 51, p. 11263. https://doi.org/10.1002/anie.201206283
13. Kasparkova, J., Kostrhunova, H., Novakova, O., et al., *Angew. Chem. Int. Ed.*, 2015, vol. 54, p. 14478. https://doi.org/10.1002/anie.201506533
14. Shi, H., Imberti, C., and Sadler, P.J., *Inorg. Chem. Front.*, 2019, vol. 6, p. 1623. https://doi.org/10.1039/C9QI00288J
15. Bellotti, P., Koy, M., Hopkinson, M.N., and Glorius, F., *Nat. Rev. Chem.*, 2021, vol. 5, p. 711. https://doi.org/10.1038/s41570-021-00321-1
16. Marion, M. and Nolan, S.P., *Acc. Chem. Res.*, 2008, vol. 41, p. 1440. https://doi.org/10.1021/ar800020y
17. Strassner, T., *Acc. Chem. Res.*, 2016, vol. 49, p. 2680. https://doi.org/10.1021/acs.accounts.6b00240
18. Sun, R.W.Y., Chow, A.L.F., Li, X.H., et al., *Chem. Sci.*, 2011, vol. 2, p. 728. https://doi.org/10.1039/C0SC00593B
19. Vishkaee, T.S., Fazaeli, R., and Yousefi, M., *Russ. J. Inorg. Chem.*, 2019, vol. 64, p. 237. https://doi.org/10.1134/S0036023619020062
20. Narayana, B.K., Keri, R.S., Hanumantharayudu, N.D., and Budagumpi, S., *Eur. J. Inorg. Chem.*, 2021, vol. 2021, p. 4349. https://doi.org/10.1002/ejic.202100258
21. Poyatos, M. and Peris, E., *Dalton Trans.* 2021, vol. 50, p. 12748. https://doi.org/10.1039/D1DT02035H
22. Nguyen, V.H., El Ali, B.M., and Huynh, H.V., *Organometallics*, 2018, vol. 37, p. 2358. https://doi.org/10.1021/acs.organomet.8b00347
23. Nayak, S. and Gaonkar, S.L., *ChemMedChem*, 2021, vol. 16, p. 1360. https://doi.org/10.1002/cmdc.202000836

24. Guarra, F., Pratesi, A., Gabbiani, C., and Biver, T., *J. Inorg. Biochem.*, 2021, vol. 217, p. 111355. https://doi.org/10.1016/j.jinorgbio.2021.111355

25. Zhao, S., Yang, Z., Jiang, G., et al., *Coord. Chem. Rev.*, 2021, vol. 449, p. 214217. https://doi.org/10.1016/j.ccr.2021.214217

26. Visbal, R. and Gimeno, M.C., *Chem. Soc. Rev.*, 2014, vol. 43, p. 3551. https://doi.org/10.1039/C3CS60466G

27. Chung, L.H., Lo, H.S., Ng, S.W., et al., *Sci. Rep.*, 2015, vol. 5, p. 15394. https://doi.org/10.1038/srep15394

28. Chang, C.F., Cheng, Y.M., Chi, Y., et al., *Angew. Chem. Int. Ed.*, 2008, vol. 47, p. 4542. https://doi.org/10.1002/anie.200800748

29. Hemmert, C. and Gornitzka, H., *Dalton Trans.*, 2015, vol. 45, p. 440. https://doi.org/10.1039/C5DT03904E

30. Becke, A.D., *J. Chem. Phys.*, 1993, vol. 98, p. 5648. https://doi.org/10.1063/1.464913

31. Perdew, J.P., Chevary, J.A., Vosko, S.H., et al., *Phys. Rev. B.*, 1992, vol. 46, p. 6671. https://doi.org/10.1103/PhysRevB.46.6671

32. Perdew, J.P., *Phys. Rev.*, 1986, vol. 33, p. 8822. https://doi.org/10.1103/PhysRevB.33.8822

33. Andrae, D., Häußermann, U., Dolg, M., et al., *Theoret. Chim. Acta.*, 1991, vol. 78, p. 247. https://doi.org/10.1007/BF01114537

34. Hay, P.J. and Wadt, W.R., *J. Chem. Phys.*, 1985, vol. 82, p. 299. https://doi.org/10.1063/1.448975

35. Krishnan, V., Binkley, J.S., Seeger, R., and Pople, J.A., *J. Chem. Phys.*, 1980, vol. 72, p. 650. https://doi.org/10.1063/1.438955

36. Luo, Y., Chen, Z., Hu, J., et al., *Phys. Chem. Chem. Phys.*, 2019, vol. 21, p. 2764. https://doi.org/10.1039/C8CP06804F

37. Lam, W.H., Lam, E.S.H., and Yam, V.W.W., *J. Am. Chem. Soc.*, 2013, vol. 135, p. 15135. https://doi.org/10.1021/ja406810a

38. Ogawa, T., Sameera, W.M.C., Saito, D., et al., *Inorg. Chem.*, 2018, vol. 57, p. 14086. https://doi.org/10.1021/acs.inorgchem.8b01654

39. Newman, C.P., Deeth, R.J., Clarkson, G.J., and Rourke, J.P., *Organometallics*, 2007, vol. 26, p. 6225. https://doi.org/10.1021/om700671y

40. Exstrom, C.L., Pomije, M.K., and Mann, K.R., *Chem. Mater.*, 1998, vol. 10, p. 942. https://doi.org/10.1021/cm970788t

41. Fan, H.W., Bai, F.Q., Zhang, Z.X., et al., *RSC Adv.*, 2017, vol. 7, p. 17368. https://doi.org/10.1039/C7RA00705A